Journal of the Korean Electrochemical Society
Vol. 27, No. 4, 2024, 169-176
https://doi.org/10.5229/JKES.2024.27.4.169

Research Paper
pISSN 1229-1935
eISSN 2288-9000

수전해 산소발생반응을 위한 전기촉매로서 Ir/Au 나노클러스터의 최적화

John Jherson Bofill · Paula Marielle Ababao · 이재원 · 홍승택 · 오일환*
금오공과대학교 응용화학과 및 에너지융합공학과

(2024년 10월 23일 접수 : 2024년 10월 31일 수정 : 2024년 11월 5일 채택)

Optimization of Ir/Au Nanoclusters as Electrocatalyst for Oxygen Evolution Reaction in Water Electrolysis

John Jherson Bofill, Paula Marielle Ababao, Jae-won Lee, Seung-taek Hong, and Ilwhan Oh*
Department of Applied Chemistry and Energy Convergence Engineering, Kumoh National Institute of Technology, Gumi, Gyeongbuk, South Korea

(Received October 23, 2024 : Revised October 31, 2024 : Accepted November 5, 2024)

초 록

산소발생반응(OER)을 위한 효율적이고 내구성 있는 전기촉매는 수전해를 통한 녹색수소 생산 기술을 발전시키는 데 필수적이다. 이리듐은 산성 환경, 특히 Proton exchange membrane (PEM) 전극에서 높은 촉매 활성과 안정성으로 선호되지만, 높은 비용과 희소성으로 인해 대규모 적용이 제한된다. 이 연구는 금 나노입자를 지지체로 사용하여 Ir 활용을 최대화하고 촉매 성능을 유지하면서 Ir의 사용량을 줄이는 것을 목표로 하였다. Ir/Au 나노클러스터(Ir/Au-NC)는 다양한 비율의 Ir을 이용해 합성되었고, 구조적, 전기화학적 및 촉매적 특성을 측정했다. 최적화된 Ir 0.6 wt%의 나노클러스터가 높은 질량 활성과 낮은 과전압 간의 균형을 달성했다. Ir/Au-NC 촉매는 일반적인 Ir-Black ($23\ m^2\ g^{-1}$)보다 상당히 더 큰 전기화학적 활성 표면적($116\ m^2\ g^{-1}$)을 나타내며, Ir-Black의 과전압 395 mV에 비해 더 낮은 347 mV의 과전압을 나타냈다. 또한 최적화된 촉매는 100회 사이클 후에도 초기 활성의 85%를 유지하여 뛰어난 안정성을 나타낸다.

Abstract : Efficient and durable electrocatalysts for the oxygen evolution reaction (OER) are essential for advancing green hydrogen production via water electrolysis. Iridium is favored for its high catalytic activity and stability in acidic environments, particularly in proton exchange membrane (PEM) electrolyzers, but its high cost and scarcity limit large-scale application. This study explores the use of gold nanoparticle supports to enhance the utilization of Ir, aiming to reduce Ir loading while maintaining catalytic performance. Ir/Au nanocluster (Ir/Au-NC) was synthesized with varying Ir loadings, and their structural, electrochemical, and catalytic properties were evaluated. An optimal Ir loading of 0.6 wt% was identified, achieving a balance between high mass activity and low overpotential. The Ir/Au-NC catalyst exhibited a significantly larger electrochemically active surface area (ECSA) of $116\ m^2\ g^{-1}$ than commercial Ir Black ($23\ m^2\ g^{-1}$), resulting in a lower overpotential of 347 mV compared to 395 mV for Ir Black. Furthermore, the optimized catalyst maintained 85% of its initial activity after 100 cycles, demonstrating excellent stability.

Keywords: Green hydrogen, Water electrolysis, Hydrogen economy, Oxygen evolution reaction, Catalysis

*E-mail: ioh@kumoh.ac.kr

1. Introduction

The global energy system is currently undergoing a critical transition, driven by the need to reduce greenhouse gas emissions and mitigate climate change. Approximately 82% of the world's energy supply still relies on fossil fuel burning, a major contributor to global warming. To achieve carbon neutrality, shifting towards a sustainable energy economy supported by renewable energy sources (RES) such as solar, wind, and nuclear is essential. However, the intermittent nature of RES demands efficient and scalable energy storage systems.[1] Hydrogen produced via water electrolysis, offers a viable solution due to its high gravimetric energy density and its ability to store excess electrical energy in the form of storable gas.[2]

Water electrolysis is a process that splits water molecules into hydrogen (H_2) and oxygen (O_2), a clean method for hydrogen production, particularly when powered by renewable electricity.[3] Among the various electrolysis technologies, Proton exchange membrane water electrolyzers (PEMWEs) are particularly attractive because of their high efficiency, compact design, and ability to produce high-purity hydrogen.[4] However, PEMWEs depend on platinum-group metals (PGMs) such as Ir and Ru as electrocatalysts to maintain performance under acidic conditions.[5] Iridium, despite its exceptional activity and stability for oxygen evolution reactions (OER), presents difficulties in large-scale applications due to its high cost and limited availability.[6,7]

To address this, research has been focused toward developing nanostructured electrocatalysts which optimizes Ir utilization while maintaining or even enhancing catalytic performance.[8] Recent advances have demonstrated that nanostructures, such as Ir-based core-shell morphologies or alloyed nanoparticles, significantly enhance the electrochemically active surface area (ECSA) and intrinsic catalytic activity by inducing lattice strain, electronic structure modulation, and facilitating synergistic interactions between materials.[9]

Gold (Au) nanoparticles have emerged as a promising support material for Ir-based OER electrocatalysts. The incorporation of Au as a substrate in bimetallic nanostructures can enhance the dispersion of Ir and optimize its catalytic properties due to the unique electronic and geometric characteristics of Au.[10] Furthermore, Au is resistant to oxidation and is capable of forming nanostructures with Ir which can improve the stability and performance of the catalyst under operational conditions.[11] Recent studies have shown that using Au as a support can lead to reduced Ir loading while maintaining high catalytic activity, offering a cost-effective approach to developing efficient electrocatalysts for PEMWEs.[12]

Optimizing the use of Ir on Au supports could significantly reduce the reliance on scarce and expensive materials in green hydrogen production. This strategy maximizes Ir efficiency, thereby lowering costs and enhancing the scalability of PEM electrolyzers, contributing to the broader development of sustainable energy solutions.[13] Despite recent progress, further research is necessary to refine synthesis techniques and understand the underlying mechanisms that enhance catalytic activity and stability.

This study aims to optimize the synthesis parameters of Ir/Au nanocluster (Ir/Au-NC) to minimize Ir loading while maximizing catalytic activity. Various Ir precursor loadings were investigated to determine their effects on the electrochemical properties and overall performance of the Ir/Au-NC electrocatalysts in OER. The findings demonstrate that an optimized Ir loading of 0.6 wt% achieves high mass activity and low overpotential, indicating that Au-supported Ir nanoclusters could provide a viable pathway for more sustainable and scalable hydrogen production technologies. Furthermore, the study compares the performance of the optimized catalysts with that of commercially available Ir-based catalysts, such as Ir Black, to evaluate their relative efficacy and stability.

2. Experimental

2.1 Materials

Gold nanopowder (Au, 99.99%, 50–100 nm) was obtained from US Research Nanomaterials Inc. (Texas, USA). Ir precursor: Iridium (IV) chloride hydrate ($IrCl_4 \cdot xH_2O$, technical grade), Sodium tetrahydridoborate ($NaBH_4$, purity ≥ 98%), and Nafion 117 solution (~5 wt%) were purchased from Sigma-

Aldrich. Isopropyl alcohol (C_3H_8O, extra pure), ethanol (C_2H_5OH, purity ≥ 94.5%), perchloric acid ($HClO_4$, purity ≥ 60%), and mercury nitrate ($Hg(NO_3)_2{\cdot}H_2O$, purity ≥ 99.9%) were supplied by Daejung Chemicals and Metals Co. (Siheung-si, South Korea).

2.2 Synthesis of Ir/Au-NC

Firstly, the Ir precursor ($IrCl{\cdot}xH_2O$) was dispersed in 50 mL of deionized water using horn sonication for 5 min. The resulting suspension was transferred to a two-necked round-bottom flask, heated to 70 ºC, and stirred at 500 rpm using an overhead Teflon paddle. Au nanoparticles were similarly dispersed in deionized water and added to the flask. Next, $NaBH_4$ was dispersed in 15 mL of isopropyl alcohol and sonicated for 1 min, then added dropwise to the flask at a rate of 3.33 mL min^{-1}. After the complete addition of the reductant, the reaction was maintained for 2 hr under continuous stirring at 70 ºC. Upon completion, the flask was placed in an ice bath for 10 min. The cooled mixture was transferred into 50 mL centrifuge tubes for washing, and centrifuged at 10,000 rpm for 10 min, and the supernatant was removed, leaving the pellet behind. This washing step was repeated twice with deionized water to ensure the removal of any unreacted chemicals. Lastly, the remaining pellet was dispersed in deionized water and dried in a vacuum oven at 90 ºC overnight. The synthesized Ir/Au-NC powder was then grounded afore characterization.

2.3 Material Characterization

The morphological characteristics of the samples were examined using Cs-corrected Scanning Transmission Electron Microscope (Cs-STEM) with a dual detector EDS, and Field Emission Scanning Electron Microscope (FE-SEM; MAIA III) equipped with an Energy Dispersive X-ray Spectroscopy (EDS) device. For these analyses, the Ir/Au-NC powder was dispersed in deionized water at a concentration of 2 mg·mL^{-1}. The suspension was deposited onto a silica substrate for SEM imaging, while a Cu grid was dipped into the solution for Cs-STEM analysis. X-ray diffraction (XRD) patterns were obtained using a Rigaku Diffractometer (SmartLab) with a Cu Kα radiation source (λ = 1.54 Å). The operating conditions included an accelerating electron voltage of 40 kV and an anode current of 40 mA. The intensity of scattered X-rays was measured with a step size of 2 min^{-1} over a 2θ range of 10–90º. To determine the chemical states present on the surface, an X-ray Photoelectron Spectrometer (XPS, PHI 5000 VersaProbe III) was employed. The parameters for XPS analysis included an Al Kα X-ray source at 150 W, a vacuum pressure below 5×10^{-8} mbar, an energy range of 40–1500 eV with a resolution of 70 eV, and a pass energy of 50 eV. The elemental percentages of Ir and Au in the synthesized samples were quantified using a Wavelength Dispersive X-ray Fluorescence Spectrometer (WD-XRF; ZSX Primus, Rigaku).

2.4 Electrochemical Characterization

2.4.1 Catalyst ink and working electrode preparation

A catalyst ink with a concentration of 0.2 mg mL^{-1} was prepared by dispersing 1 mg of the Ir/Au-NC in a mixture containing 3.80 mL of deionized water, 1.20 mL of isopropyl alcohol, and 20 μL of Nafion 117 solution. The mixture was sonicated for 10 min to ensure proper dispersion of the catalyst. A 3 mm diameter Au working electrode was polished using a 0.3 μm Al_2O_3 polishing suspension until a mirror-like surface was achieved. Subsequently, 10 μL of the prepared catalyst ink was deposited onto the electrode and dried at 70 ºC for 2.5 min.

2.4.2 Linear sweep voltammetry

Linear sweep voltammetry (LSV) was conducted using a three-electrode setup connected to an SP-150 Potentiostat (BioLogic, France). The working electrode was a 3 mm Au rotating disk electrode (RDE), the reference electrode was a saturated calomel electrode (SCE), and the counter electrode was a platinum mesh. A 0.1 M $HClO_4$ solution served as the electrolyte. Initially, 10 no-current cycles were performed using the Current Interrupt (CI) technique at a compensation level of 80%, ranging from –2.5 to 2.5 V. The catalysts were conditioned with 19 LSV cycles from 1.30 V to 1.70 V versus the Reversible Hydrogen Electrode (RHE) at a scan rate of 50 mV s^{-1}, after which the 20th cycle was recorded at a scan rate of 20 mV s^{-1}.

2.4.3 Mercury underpotential deposition

The electrochemically active surface area (ECSA) was measured using the mercury underpotential deposition (Hg UPD) technique.[14,15] This process utilized the same three-electrode configuration but with a 1.0 M $HClO_4$ solution containing 1 mM $Hg(NO_3)_2$ as the electrolyte. The measurement involved applying the Current Interrupt (CI) protocol, followed by a series of cyclic voltammetry (CV) scans over a potential range of 0.5 to 0.9 V versus the Reversible Hydrogen Electrode (RHE) at scan rates ranging from 60 to 5 mV s^{-1}.

3. Results and Discussion

In Fig. 1(a,b), the characterization of pristine gold nanoparticles (AuNPs) and the iridium-impregnated gold nanoclusters (Ir/Au-NC) through TEM analysis showed that both AuNP and Ir/Au-NC are aggregates of smaller nanoparticles (2–3 nm), which can potentially contain a high density of active sites.[16] In Fig. 1(c), the HAADF-EDS reveals a uniform distribution of Ir on the Au-NC, suggesting the Ir has been successfully impregnated onto the Au support.

XRD patterns of the synthesized Ir/Au-NC in Fig. 2 reveal important structural information regarding the interaction between Ir and Au lattices. Notably, no distinct peaks corresponding to Ir were observed in any of the XRD patterns. Absence of Ir peaks is attributed to the relatively low loading and less ordered structure of Ir, making it undetectable by XRD,[17] suggesting that the Ir is highly dispersed and present partially in an amorphous state rather well-ordered crystalline domain.

Furthermore, upon impregnation with Ir, all principal Au peaks in the XRD pattern series shifted into higher 2θ values relative to pristine AuNP, indicating lattice compression of the Au crystals. The magnified view of the principal Au (111) peak in Fig. 2 further highlights the positive shifting of the Au (111) peak in the Ir/Au-NC ($\Delta \approx 0.02°$), and confirms strain induced by the Ir loading.[18] Ir has a smaller d-spacing compared to Au; there-

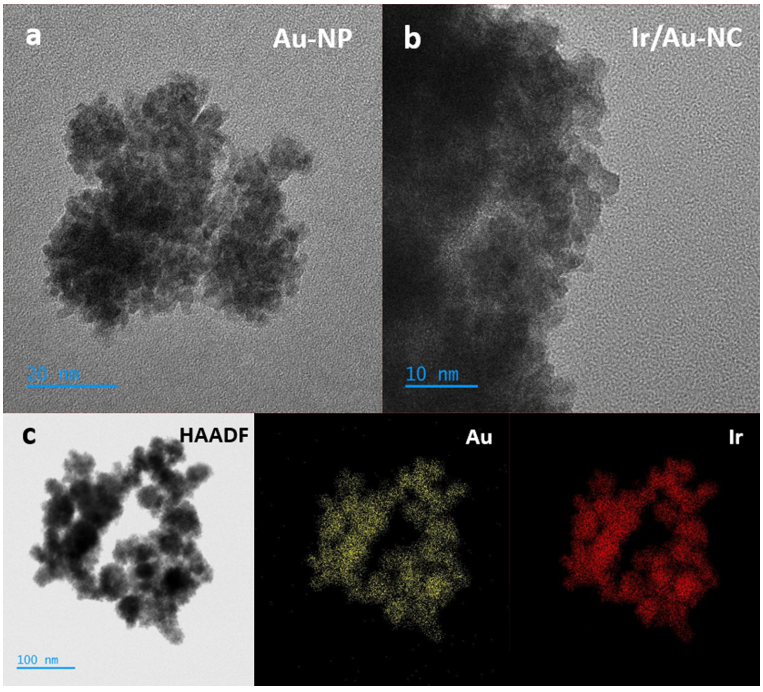

Fig. 1. (a) TEM image of gold nanoparticles (AuNP). (b) Magnified TEM image of synthesized Ir/Au-NC. (c) High-Angle Annular Dark-Field (HAADF) image and Energy Dispersive Spectroscopy (EDS) elemental mapping of Au (yellow) and Ir (red), showing the random distribution of Au and Ir.

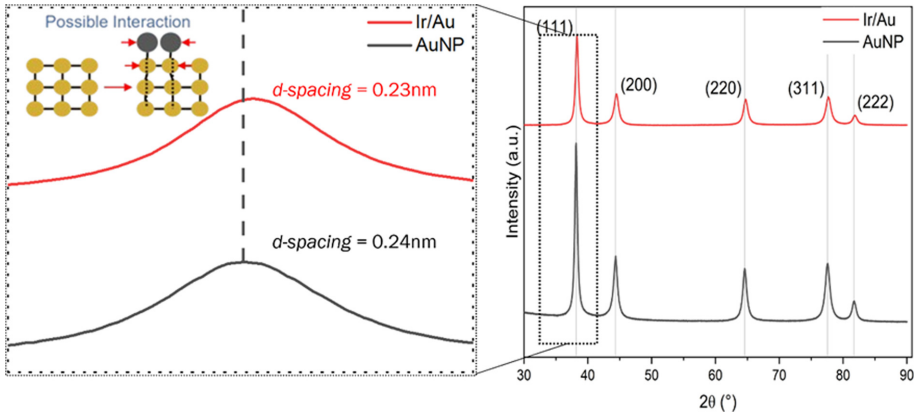

Fig. 2. XRD spectra of pristine AuNP and synthesized Ir/Au (right). Magnified view of the principal peak [Au (111)] from the highlighted area, with an inset showing possible interaction, lattice constant values of Ir/Au and Au (left).

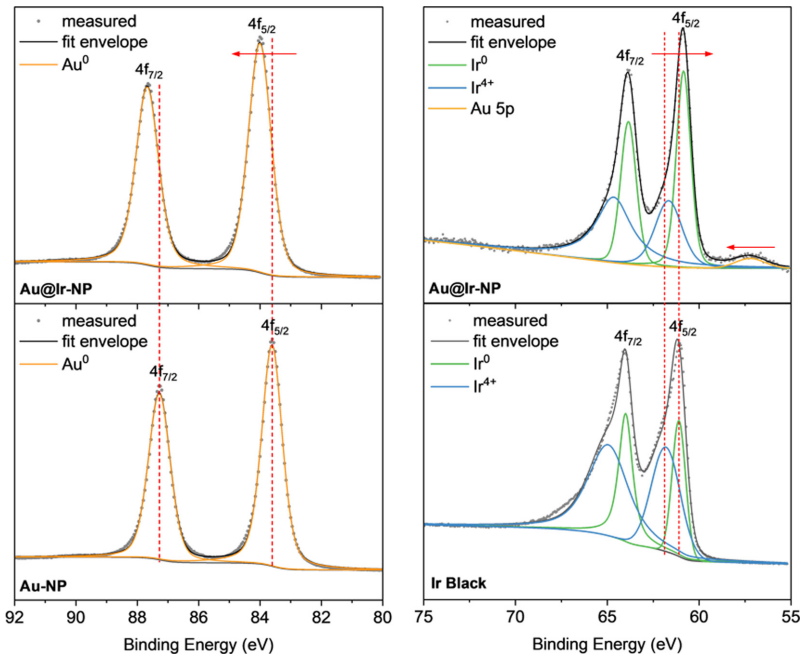

Fig. 3. (a) XPS spectra of the Au 4f region for Ir/Au-NC (top) and Au-NP (bottom), showing measured data, fit envelope, and Au^0 component. (b) XPS spectra of the Ir 4f region for Ir/Au-NC (top) and Ir Black (bottom), displaying measured data, fit envelope, Ir^0, Ir^{4+} components, and Au 5p.

fore, when Ir is deposited onto the surface of Au nanoparticles, it exerts a compressive force on the Au lattice, resulting in a reduction of the Au d-spacing. Overall, the findings demonstrate that the impregnation of Ir into Au leads to significant lattice strain, creating a junction between Au crystal structure and Ir presence.[19,20)]

XPS analysis was carried out to examine the compositional and chemical states of the Ir/Au-NC. The Au 4f spectrum in Fig. 3 shows two prominent peaks at 84.0 eV and 87.7 eV, corresponding to Au^o within the Ir/Au-NC structure. These binding energies are slightly higher than those of the pure Au reference, which appear at 83.6 eV and

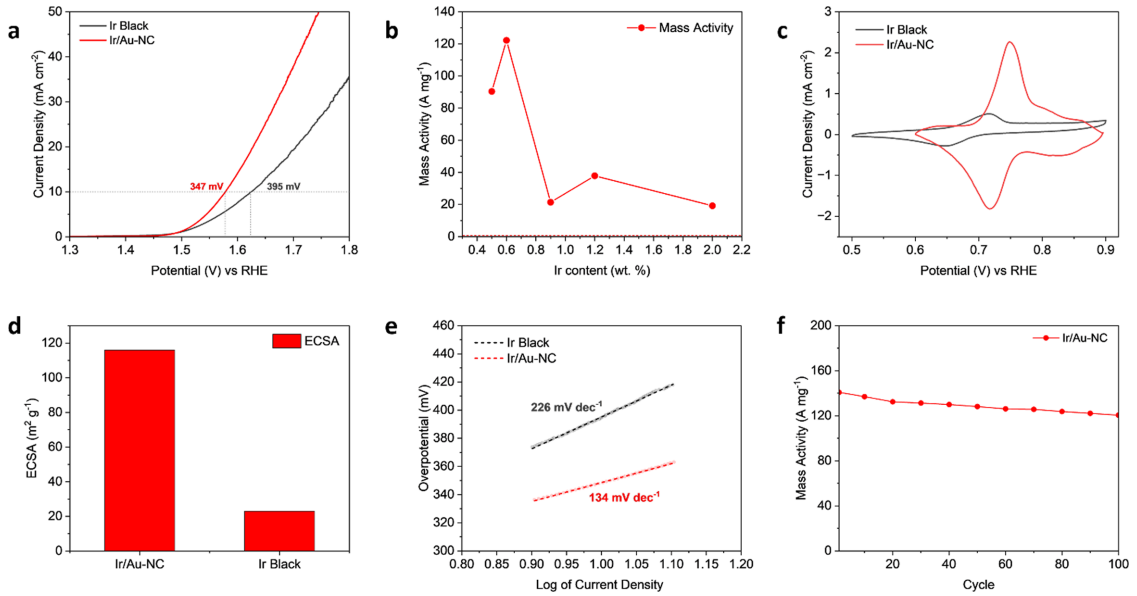

Fig. 4. (a) LSV curves of Ir/Au-NC (0.6 wt% Ir) and Ir Black in 0.1 M $HClO_4$. (b) Mass activity as a function of Ir content (wt% Ir) in Ir/Au-NC, with the final product ratio of Ir content determined using XRF. The reference line represents the performance of commercial Ir Black. (c) Hg UPD CV curves representing the ECSA of Ir/Au-NC and Ir Black. (d) Bar chart comparing the ECSA of Ir/Au-NC (0.6 wt% Ir) and Ir Black. (e) Tafel plots for Ir/Au-NC (0.6 wt% Ir) and Ir Black, highlighting differences in OER kinetics. (f) Stability test of Ir/Au-NC (0.6 wt% Ir) over 100 cycles in 0.1 M $HClO_4$.

87.3 eV, respectively. The observed positive shift for Au^o in the Ir/Au-NC structure indicates a reduction in electron density around the Au core, likely caused by electronic redistribution between the Au core and the Ir shell.

Meanwhile, Ir 4f spectrum for Ir/Au-NC reveals peaks at 60.8 eV and 61.6 eV for Ir^o, and at 63.9 eV and 64.7 eV for Ir^{4+}. Note that both Ir^o (−0.3 eV) and Ir^{4+} (−0.4 eV) are negative shifted compared to those for Ir Black, which suggests an electronic donation from the Au core to the Ir adlayer. Furthermore, the existence of Ir^{4+} peaks suggest that the Ir shell is partially oxidized, forming an IrO_2 layer, which is regarded as providing active sites for OER.

Optimizing Ir loading in the Ir/Au-NC catalyst reveals a clear relationship between mass activity and Ir surface coverage. As shown in Fig. 4(a), the Ir/Au-NC catalyst with an Ir content of 0.6 wt%, measured from the final product ratio, achieves a significantly lower overpotential of 347 mV compared to 395 mV for commercial Ir Black in 0.1 M $HClO_4$, indicating enhanced OER efficiency. This improved performance is attributed to the impregnation of Ir onto the Au support, which increases the accessibility of active sites and enhances catalytic properties.[21)]

Examining mass activity as a function of Ir content in Fig. 4(b) reveals that the optimal performance is achieved at an Ir loading of 0.6 wt%, with the highest recorded mass activity of 122 A mg^{-1}. This peak mass activity possibly results from an ideal dispersion and interaction of Ir particles on the Au support, which enhances the accessibility and availability of active sites for OER. At this optimal loading, the structure of Ir/Au-NC appears to facilitate efficient electron transfer and catalytic reactions, maximizing activity. Increasing the Ir content beyond 0.6 wt% leads to a decline in mass activity, possibly due to agglomeration effects that reduce the efficiency of catalytic interactions. Therefore, the 0.6 wt% Ir loading provides the most favorable balance, achieving maximum catalytic performance.

Hg UPD CV curves in Fig. 4(c) represent ECSA,

with Ir/Au-NC displaying a larger peak area compared to Ir Black, suggesting a greater number of accessible active sites. This enhanced ECSA is quantified in Fig. 4(d), showing that Ir/Au-NC achieves an ECSA of 116 $m^2 g^{-1}$, significantly higher than the 23 $m^2 g^{-1}$ observed for Ir Black. This large ECSA value for Ir/Au-NC highlights its superior structure, allowing for greater active site exposure and contributing to its higher mass activity in OER applications. In contrast, the lower ECSA of Ir Black reflects limited active site accessibility, resulting in reduced catalytic performance.

Tafel plots in Fig. 4(e) reveals Tafel slopes of 134 mV dec^{-1} for Ir/Au-NC and 226 mV dec^{-1} for Ir Black. The lower Tafel slope of Ir/Au-NC indicates more favorable kinetics for the OER compared to commercial Ir Black. This suggests that the unique impregnation of Ir on the Au support in Ir/Au-NC facilitates a more efficient charge transfer process, enhancing the catalytic performance during OER.

Stability experiments were conducted to evaluate the long-term performance of the catalysts. Fig. 4(f) displays the stability test of the Ir/Au-NC catalyst in 0.1 M $HClO_4$ electrolyte, where it exhibited a ~15% loss in activity after 100 CV cycles. This decline suggests some degradation over time, likely due to partial dissolution or structural changes in the catalyst, which can impact the accessibility of active sites. Nonetheless, the relatively modest decrease in activity indicates that Ir/Au-NC retains a significant portion of its performance over repeated cycling, making it a promising candidate for practical applications in PEM water electrolysis.

4. Conclusions

This study successfully optimized the synthesis parameters for Ir/Au-NC catalysts by adjusting Ir precursor loading to enhance OER performance while minimizing the use of precious Ir. The results indicate that an Ir loading of 0.6 wt% provides an optimal balance, achieving the highest mass activity of 122 A mg^{-1}, a low overpotential of 347 mV, a substantial ECSA of 116 $m^2 g^{-1}$, and a favorable Tafel slope of 134 mV dec^{-1}. The high ECSA reflects an abundance of accessible active sites due to the well-dispersed Ir structure on the Au support, while the lower Tafel slope indicates improved OER kinetics, suggesting efficient charge transfer during the reaction. The optimized Ir/Au-NC catalyst outperformed commercial Ir Black and demonstrated excellent stability, retaining approximately 85% of its initial activity after 100 cycles. These findings underscore the potential of Ir/Au-NC catalysts as a cost-effective and efficient alternative for sustainable hydrogen production in PEM electrolyzers.

Acknowledgments

This research was supported by the academic research fund from the Kumoh National Institute of Technology (2022~2024).

References

1. M. Noussan, P. P. Raimondi, R. Scita, and M. Hafner, The role of green and blue hydrogen in the energy transition—a technological and geopolitical perspective, *Sustainability*, **13(1)**, 298 (2021).
2. S. Wang, A. Lu, and C.-J. Zhong, Hydrogen production from water electrolysis: Role of catalysts, *Nano Convergence*, **8**, 4 (2021).
3. T. Schuler, T. Kimura, T. J. Schmidt, and F. N. Büchi, Towards a generic understanding of oxygen Evolution reaction kinetics in polymer electrolyte water electrolysis, *Energy Environ. Sci.*, **13(7)**, 2153–2166 (2020).
4. A. Grimaud, A. Demortière, M. Saubanère, W. Dachraoui, M. Duchamp, M.-L. Doublet, and J.-M. Tarascon, Activation of surface oxygen sites on an iridium-based model catalyst for the oxygen evolution reaction, *Nat. Energy*, **2**, 16189 (2016).
5. S. Cherevko, A. R. Zeradjanin, G. P. Keeley, and K. J. J. Mayrhofer, A comparative study on gold and platinum dissolution in acidic and alkaline media, *J. Electrochem. Soc.*, **161(12)**, H822 (2014).
6. H. Okamoto and T. B. Massalski, The Au-Ir (gold-iridium) system, *Bull. Alloy Phase Diagr.*, **5(4)**, 381 (1984).
7. J. Park, Y. J. Sa, H. Baik, S. H. Joo, and K. Lee, Iridium-based multimetallic nanoframe@nanoframe structure: An efficient and robust electrocatalyst toward oxygen evolution reaction, *ACS Nano*, **11(6)**, 5500–5509 (2017).
8. T. Reier, M. Oezaslan, and P. Strasser, Electrocatalytic oxygen evolution reaction (OER) on Ru, Ir, and Pt catalysts: A comparative study of nanoparticles and bulk materials, *ACS Catal.*, **2(8)**, 1765–1772 (2012).
9. E. Westsson, S. Picken, and G. Koper, The effect of lattice strain on catalytic activity, *Chem. Commun.*, **55(9)**, 1338–1341 (2019).
10. A. M. Oliveira, R. R. Beswick, and Y. Yan, A green hydrogen economy for a renewable energy society, *Curr.*

Opin. Chem. Eng., **33**, 100701 (2021).
11. B. M. Tackett, W. sheng, S. Kattel, S. Yao, B. Yan, K. A. Kuttiyiel, Q. Wu, and J. G. Chen, Reducing iridium loading in oxygen evolution reaction electrocatalysts using core–shell particles with nitride cores, *ACS Catal.*, **8(3)**, 2615–2621 (2018).
12. A. L. Strickler, M. Escudero-Escribano, and T. F. Jaramillo, Core–shell Au@metal-oxide nanoparticle electrocatalysts for enhanced oxygen evolution, *Nano Lett.*, **17(10)**, 6040–6046 (2017).
13. S. M. Alia, S. Shulda, C. Ngo, S. Pylypenko, and B. S. Pivovar, Iridium-based nanowires as highly active, oxygen evolution reaction electrocatalysts, *ACS Catal.*, **8(3)**, 2111–2120 (2018).
14. S. M. Alia, K. E. Hurst, S. S. Kocha, and B. S. Pivovar, Mercury underpotential deposition to determine iridium and iridium oxide electrochemical surface areas, *J. Electrochem. Soc.*, **163(11)**, F3051 (2016).
15. T. Nagai, Z. Siroma, T. Akita, and T. Ioroi, Electrochemical quartz crystal microbalance study of underpotential deposition of mercury on iridium metal and iridium oxide, *Electroanalysis*, e202400154 (2024).
16. H. Wang, Z. Chen, D. Wu, M. Cao, F. Sun, H. Zhang, H. You, W. Zhuang, and R. Cao, Significantly enhanced overall water splitting performance by partial oxidation of Ir through Au modification in core–shell alloy structure, *J. Am. Chem. Soc.*, **143(12)**, 4639–4645 (2021).
17. B. D. Cullity and R. Smoluchowski, Elements of X-ray diffraction, *Phys. Today*, **10(3)**, 50 (1957).
18. G. J. M. Koper, *An Introduction to Interfacial Engineering*, 1st ed., VSSD, Delft, Netherlands (2007, corrected 2009, 2011).
19. B. T. Sneed, A. P. Young, and C.-K. Tsung, Building up strain in colloidal metal nanoparticle catalysts, *Nanoscale*, **7(29)**, 12248–12265 (2015).
20. M. Jørgensen and H. Grönbeck, Perspectives on computational catalysis for metal nanoparticles, *ACS Catal.*, **9(10)**, 8872–8881 (2019).
21. Z. Ke, L. Li, Q. Jia, Y. Yang, and H. Cui, Facile synthesis of jagged Au/Ir nanochains with superior electrocatalytic activity for oxygen evolution reaction, *Appl. Surf. Sci.*, **463**, 58–65 (2019).
22. R. Jin and T. Higaki, Open questions on the transition between nanoscale and bulk properties of metals, *Commun. Chem.*, **4**, 28 (2021).